*metals*

MDPI

*Article*

# Numerical Simulation of Electromagnetic Field in Slab Electroslag Remelting Process with Double Electrode Series

**Qi Li [1,2], Zhenquan Jing [1] and Yanhui Sun [1,*]**

[1] Collaborative Innovation Center of Steel Technology, University of Science and Technology Beijing, Beijing 100083, China
[2] Shanghai Electric SHMP Casting & Forging Co., Ltd., Shanghai 200245, China
* Correspondence: sun_yanhui@163.com

**Abstract:** In this paper, a mathematical model of an electromagnetic field during an electroslag remelting process of industrial-scale slab was established using a Maxwell 3D module in Ansys Electromagnetics Suite. The distribution characteristics of the magnetic field intensity, current density and Joule heat density during the electroslag remelting process were analyzed in detail. On this basis, the influence of the current frequency on the electroslag remelting process of an industrial scale is studied, and the influence of process parameters such as the slag pool depth, electrode insertion depth and ingot height on the electromagnetic field is also considered. The results show that the Joule heat generated in the slag pool is much greater than that of the electrode and the ingot. The maximum Joule heat is located at the contact between the electrode corner and the slag pool, and the Joule heat near the middle of the two electrodes is greater than the rest. With the increase in the current frequency, the current density distribution in the slag cell is basically unchanged. The current density inside the two electrodes increases obviously with the current frequency. When the current frequency increases from 10 Hz to 50 Hz, the maximum current density at the inner surface of the electrode increases by 14.7%. The current distribution at the lower side of the electrode in the slag pool is relatively uniform, and the current density in this region decreases with the increase in the height of the slag pool and the increase in the depth of the electrode inserted into the slag pool.

**Keywords:** electroslag remelting; double electrode series; electromagnetic field; numerical simulation

check for updates

**Citation:** Li, Q.; Jing, Z.; Sun, Y. Numerical Simulation of Electromagnetic Field in Slab Electroslag Remelting Process with Double Electrode Series. *Metals* **2024**, *14*, 37. https://doi.org/10.3390/met14010037

Academic Editor: Diego Celentano

Received: 15 November 2023
Revised: 20 December 2023
Accepted: 22 December 2023
Published: 28 December 2023

**Copyright:** © 2023 by the authors. Licensee MDPI, Basel, Switzerland. This article is an open access article distributed under the terms and conditions of the Creative Commons Attribution (CC BY) license (https://creativecommons.org/licenses/by/4.0/).

## 1. Introduction

The electroslag remelting process is to insert the metal processed into a specific shape as a consumable electrode into a conductive and refining slag pool and use the heat released by the current through the high-resistivity slag pool to melt the electrode. The molten metal droplets fall into the mold through the slag pool to form a metal molten pool. As the electrode continues to melt, the metal molten pool continues to solidify from the bottom to the top in the mold to form an ingot [1,2]. In the process of metal droplet formation and passing through the slag pool, the specific surface area of the metal droplet increases greatly, and the harmful impurity elements and non-metallic inclusions in the molten metal are quickly removed. At the same time, the smelting environment of the molten slag and non-refractory materials effectively avoids the secondary pollution of molten metals. Because a layer of slag shell is formed between the mold wall and the ingot, the lubrication between the ingot and the mold wall can be increased, and the surface quality of the ingot can be improved. The formation of the slag shell also reduces the heat loss in the radial direction of the ingot, which is beneficial to the formation of the directional solidification structure and improves its internal quality [1–4]. In addition, the electroslag remelting process is simple in operation, is low in equipment investment and operating costs and can produce ingots of different shapes. The electroslag remelting process plays an increasingly important role in the field of special metallurgy [5].

Nuclear power steel 18MND5 is a special structural steel, mainly used in a major nuclear power plant pressure vessel cylinder, water supply pipe, manhole seat, manhole cover and other components. The steel used for nuclear power needs to have the characteristics of an accurate and stable composition, fewer inclusions and a lower gas content, good mechanical properties and a metallographic structure [6,7]. In order to ensure product quality and meet the requirements of large-scale ingot, the electroslag remelting process is adopted to refine the slab produced by the continuous casting process on the basis of a series of advanced smelting technologies. Combined with the characteristics of the electrode material and product shape, a bipolar series electroslag furnace is used for production [8–11]. The physical phenomena in the electroslag remelting process are very complicated, and there is a complex interaction between the electromagnetic field, flow field and temperature field. The interaction of the electromagnetic field provides the heat required for electrode melting in the electroslag remelting process and has an important influence on the temperature change and the solidification structure of the final ingot. Therefore, it is very important to study the changes in the electromagnetic field and temperature field in the process of electroslag remelting, optimize the process of electroslag remelting and obtain high-quality ingot [12–23].

The electromagnetic field of the electroslag remelting process has been studied by many researchers. Liu F et al. [24] studied the electromagnetic behavior in the ESR process by numerical simulation and analyzed the distribution characteristics of the current density, magnetic field intensity, electromagnetic force and Joule heat in the ESR process of a laboratory and industrial scale. Wang F et al. [25] took the electrode, slag pool and ingot in the electroslag remelting process as research objects, established a finite element model of an electromagnetic field and analyzed the distribution of the magnetic field, electromagnetic force, current density and Joule heat density. Liu Y et al. [26] obtained the distribution of an electromagnetic field and joule heat field in the stable electroslag remelting process by using finite element analysis software and analyzed the distribution of the shape, temperature and velocity field of the metal melt pool in the process of electroslag remelting under basic control parameters. Jing X et al. [27,28] established a mathematical model of the electroslag remelting of hollow ingot by conducting a crystallizer, calculated the influence of different power supply methods on the temperature field of an electroslag remelting hollow ingot system and then analyzed the influence of the electric field system and temperature field distribution on the quality of the hollow ingot. Wang C et al. [29,30] analyzed the effects of the remelting current, filling ratio, electrode immersion depth and slag thickness on the solidification process of electroslag remelting. However, the electromagnetic field of the slab bipolar series electroslag remelting process lacks systematic research.

At present, however, due to the high cost of an electroslag remelting test, it is difficult to systematically study the mechanism of electroslag remelting by test methods, and most studies focus on the simple single-pole electroslag remelting of small ingot, while few studies focus on the bipolar series electroslag remelting of a large slab. Numerical simulations can overcome the defects of physical tests and are becoming an effective means to study the mechanism of electroslag remelting and establish the internal relationship between the parameters of the electroslag remelting process and the quality of the final ingot [30–32]. In this paper, a mathematical model of an electromagnetic field during the electroslag remelting process of an industrial-scale slab was established using the Maxwell 3D module in Ansys Electromagnetics Suite. The distribution characteristics of the magnetic field intensity, current density and Joule heat density during the electroslag remelting process were analyzed in detail. On this basis, the influence of the current frequency on the electroslag remelting process of an industrial scale is studied, and the influence of process parameters such as the slag pool depth, electrode insertion depth and ingot height on the electromagnetic field is also considered.

## 2. Mathematical Model

The slab bipolar series electroslag remelting model (as shown in Figure 1) is mainly composed of two electrodes, a slag pool and ingot. Single-phase AC current flows in from one electrode and out from the other, thus generating an electromagnetic field and thermal effect in the model.

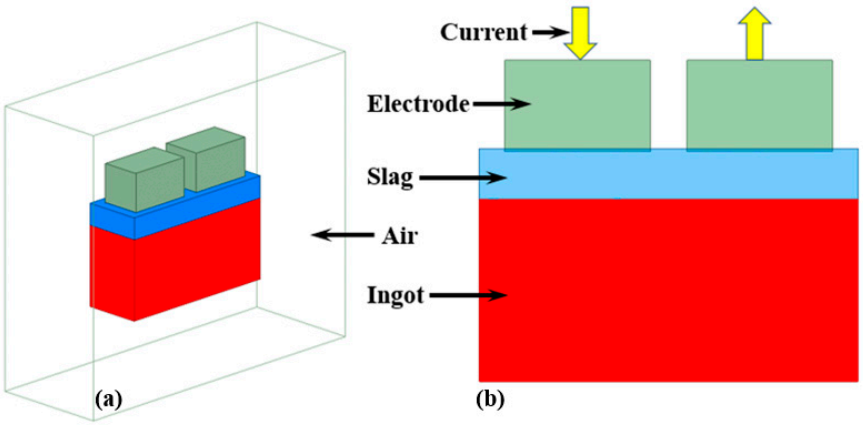



**Figure 1.** Schematic diagram of an electromagnetic field calculation model for slab electroslag remelting with a double electrode series. (**a**) General model diagram. (**b**) Longitudinal section of model.

The governing equations of an electromagnetic field are mainly described by Maxwell equations, and the thermal effect obeys Joule's law.

### *2.1. Governing Equations*

The main equations used in the model were as follows:
Gauss's law:

$$\nabla \times B = 0 \tag{1}$$

Ampere's law:

$$J = \nabla \times \frac{B}{\mu} \tag{2}$$

Faraday's law:

$$\nabla \times E = -\frac{\partial B}{\partial t} \tag{3}$$

Ohm's law:

$$J = \sigma E \tag{4}$$

Joule's law:

$$Q = \frac{|J|^2}{\sigma} \tag{5}$$

where $B$ is the magnetic flux density, T; $J$ is the induced current density, A·m$^{-2}$; $\mu$ is the magnetic permeability, H·m$^{-1}$; $E$ is the electric field strength, V·m$^{-1}$; $\sigma$ is the electrical conductivity, S·m$^{-1}$; $Q$ is the joule heat density, W·m$^{-3}$.

### *2.2. Assumptions and Simplified Mathematic Model*

To simplify the model reasonably, the following assumptions are made:

(1) The electroslag remelting process is regarded as a quasi-steady state process, and the influence of droplet movement on the electromagnetic field is ignored;
(2) Compared with the magnetic field generated by the melting current, the induced magnetic field generated in the ingot melting pool is negligible;
(3) The surface of a slag pool and molten steel pool is assumed to be flat, and the influence of the molten pool flow on the magnetic field is ignored;

(4) It is assumed that the slag film between the mold and the ingot has a good insulation effect; since the relative permeability of the mold and the cooling water is close to 1, the model is treated according to the air domain;
(5) The slag pool, ingot and electrode are regarded as isotropic materials, and their physical property parameters such as conductivity and permeability are set as constant.

### *2.3. Boundary Conditions and Calculating Parameters*

(1) The magnetic field lines are parallel to the outer surface of the air region;
(2) There are two electrodes, one positive and the other negative, and the melting current is loaded at the top of the electrode.

The electromagnetic field calculation model of slab bipolar series electroslag remelting mainly includes electrodes, a slag pool, ingot and an air domain. The electrode and ingot are titanium alloy, and the slag pool is an ANF-6 (70%$CaF_2$–30%$Al_2O_3$) slag system. Its structure is shown in Figure 1, where Figure 1a is the entire model and Figure 1b is the forward longitudinal section of the model (excluding the air domain).

In this paper, the Maxwell3D module in Ansys Electromagnetics Suite was used for the calculation. Tetrahedral mesh was used in the calculation domain, mesh adaptive technology was used for mesh encryption and more fine mesh was used for the electrodes, slag pools and ingots to improve the calculation accuracy. Detailed parameters of the model are shown in Table 1, and the physical property parameters used in the model calculation are shown in Table 2.

**Table 1.** Calculation parameters of the electromagnetic field model.

| Parameter | Value |
|---|---|
| Ingot size/mm | 2080 × 730 × 1000 |
| Slag pool size/mm | 2080 × 730 × 275 |
| Electrode sizer/mm | 800 × 500 × 500 |
| Distance between two electrodes/mm | 200 |
| Electrode insertion depth of the slag pool/mm | 15 |
| Melting current Im/kA | 20 |
| Current frequency/Hz | 50 |

**Table 2.** Electromagnetic physical property parameters of materials.

| Material | Value | |
|---|---|---|
| | Bulk Conductivity | Relative Permeability |
| Ingot, electrode | $7.14 \times 10^5$ | 1 |
| Slag pool | 175 | 1 |
| Air domain | 0 | 1 |

## 3. Model Validation

In the actual production process, the physical quantities such as the current and temperature around the model are difficult to measure, but the magnetic field can be measured in a non-contact manner using a Gaussian meter. Figure 2 shows the distribution of the magnetic field strength on the positive longitudinal section of the model under the condition of a melting current of 20 kA and a frequency of 50 Hz. It can be seen from the figure that the magnetic field is mainly distributed in the electrode, the slag pool and the top of the ingot, and the magnetic field in most of the lower part of the ingot is very small. The magnetic field intensity in the electrode is mainly distributed on the surface, and the magnetic field intensity in the slag pool is mainly distributed in the central region, which is related to the distribution of current. According to the right-hand rule, it can be judged that the magnetic field intensity in the middle area of the two electrodes is the largest due to the superposition of the magnetic field generated by the two electrodes.

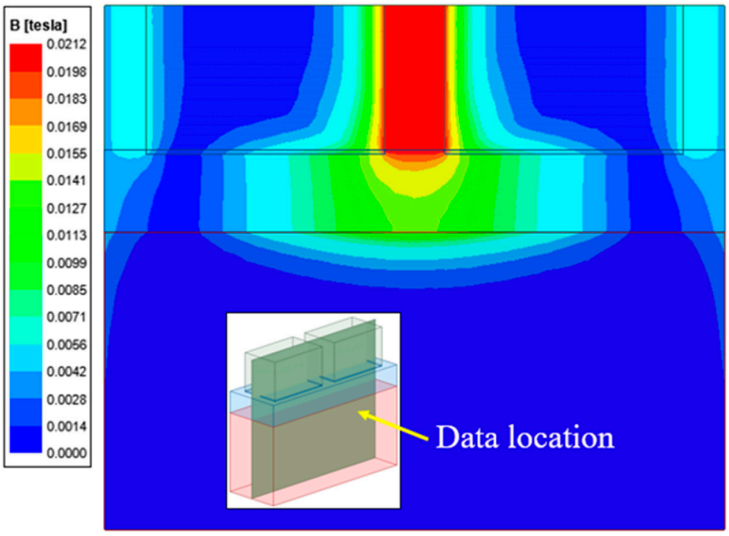



**Figure 2.** Distribution of magnetic field intensity on the forward longitudinal section of the model.

In order to compare the difference between the calculation results of the stirring magnetic field and the actual data in the field, the Gauss meter is used to measure the magnetic field strength along the two ends and the middle gap of the two electrodes on the transverse center line of the upper surface of the slag pool. Figure 3 is the comparison between the calculated value and the measured value of the magnetic field strength on the transverse center line of the upper surface of the slag pool under the melting current of 20 kA and the frequency of 50 Hz. It can be seen from the figure that the calculated value is basically consistent with the measured value, and the error is small. Table 3 shows the comparison between the measured value and the calculated value of the magnetic field strength. It can be seen that the error at X = −1000 mm is relatively large, which is 4.61%, still less than 5%. The measured value is slightly lower than the calculated value, which may be due to the existence of a certain magnetic flux leakage in the actual circuit, and some equipment is simplified in the model.

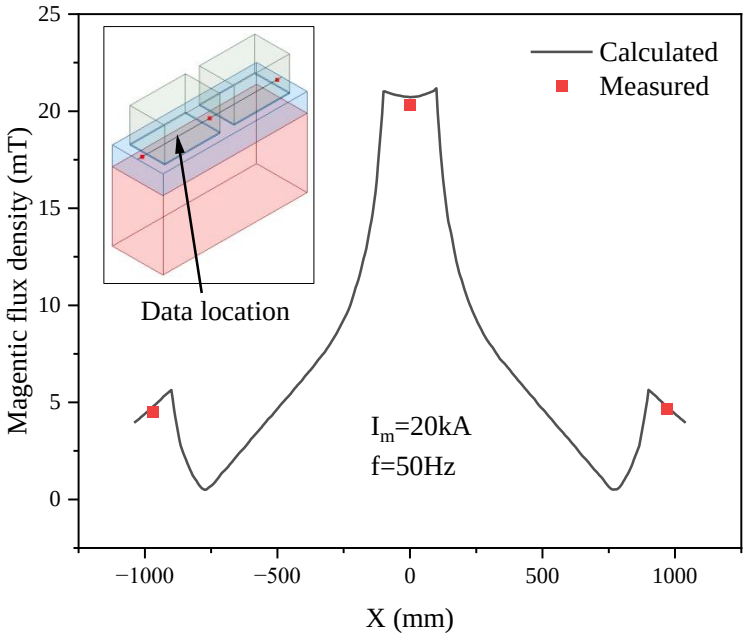



**Figure 3.** Comparison between the calculated and measured values of magnetic field intensity on the transverse center line of the upper surface of the slag pool.

**Table 3.** Comparison between the calculated and measured values of magnetic field intensity.

| Item | Position | | |
|---|---|---|---|
| | X = −1000 mm | X = 0 mm | X = 1000 mm |
| Calculated/mT | 4.77 | 20.72 | 4.78 |
| Measured/mT | 4.56 | 20.35 | 4.65 |
| Error/% | 4.61 | 1.82 | 2.80 |

## 4. Results and Discussion

### *4.1. Current Distribution in the Model*

Figure 4 shows the current distribution on the positive longitudinal section of the electroslag remelting system and the cross-section of the upper surface of the slag pool (H = 1275 mm) when the smelting current is 20 kA and the frequency is 50 Hz. It can be seen from the figure that the current flows in from the top of the left electrode and enters the slag pool through the bottom of the electrode. Due to the low conductivity of the slag pool, a part of the current enters the ingot after passing through the slag pool and finally flows out from the right electrode. The current distribution in the slag pool is relatively uniform, and the current density in the slag pool is smaller than that of the electrode and the ingot. In the electrode region, the current is mainly concentrated on the outer surface, and the skin effect is significant. Because the current directions in the two electrodes are opposite, they attract each other, and the current is concentrated in the middle region of the two electrodes, resulting in an asymmetric current distribution in the electrode. When the current enters the slag pool, the current density distribution changes due to the change in conductivity. The current density at the corner of the electrode is the largest, up to $2.6 \times 10^5$ A/m$^2$, which is much larger than that in other regions. According to the distribution of the current, it can be preliminarily judged that the middle area of the two electrodes and the slag pool near the corner of the electrode are the main heat source areas for the melting of the consumable electrode.

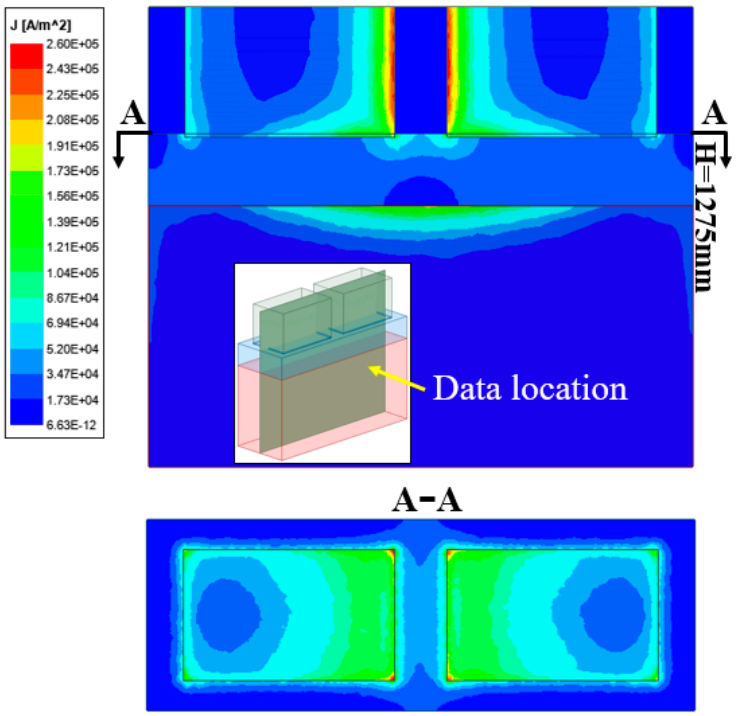



**Figure 4.** The current distribution on the vertical section of the model and the cross-section of the upper surface of the slag pool (H = 1275 mm).

### *4.2. Joule Heat Distribution in the Model*

Figure 5 shows the Joule heat distribution of the forward longitudinal section of the electroslag remelting system when the melting current is 20 kA and the frequency is 50 Hz. In order to observe the Joule heat distribution in the slag pool, the Joule heat distribution on the cross-section of 20 mm (H = 1250 mm) from the upper surface of the slag pool is also extracted. It can be seen from the figure that since the resistivity of the slag pool is much larger than that of the electrode and the ingot, although the current density in the slag pool is smaller than that of the electrode and the ingot, the Joule heat generated in the slag pool is much larger than that of the electrode and the ingot, so the Joule heat in the electrode and the ingot can be ignored. When the current enters the slag pool through the electrode, the current density at the contact between the corner and the slag pool is the largest, and the maximum Joule heat is located at the contact between the corner of the electrode and the slag pool. The Joule heat density can reach 6.98 $\times$ 107 W/m$^3$, and the Joule heat in the middle of the two electrodes is greater than that in the other parts, which makes the corner of the electrode melt first under the action of the Joule heat generated by the slag pool. More Joule heat is generated in the middle area of the slag pool, which will lead to a higher temperature in the middle area of the slag pool.

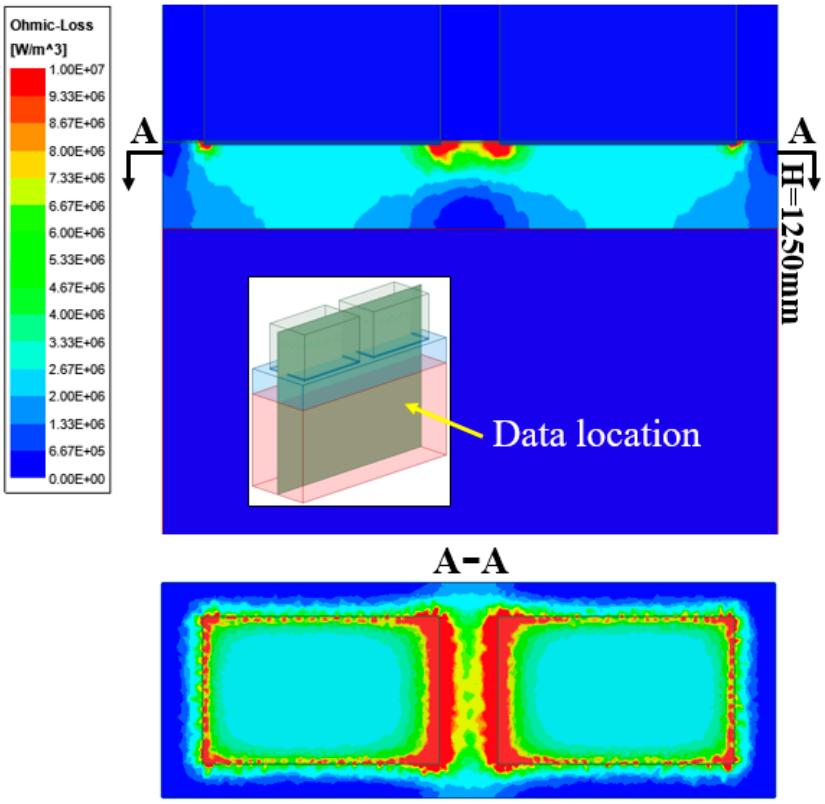



**Figure 5.** The Joule heat distribution on the vertical section of the model and the cross-section of 20 mm (H = 1250 mm) from the upper surface of the slag pool.

According to the above, the Joule heat generated in the slag pool has a very important influence on the electrode melting and the solidification process of the ingot. According to the relationship between the Joule heat and current (5), the Joule heat is mainly affected by the current density and slag pool conductivity. Due to the small change in conductivity, the current becomes the decisive factor for the generation of Joule heat. Figure 6 shows the current distribution on the positive longitudinal section of the slag pool. Compared with Figure 5, it can be seen that the distribution of Joule heat generated in the slag pool is basically the same as the current distribution. At the same time, the magnetic field generated by the electroslag remelting system is also mainly affected by the smelting

current. It can be seen that the distribution of current density is the main influencing factor of the electromagnetic field of the whole system. In order to grasp the main contradiction, the influence of the change in the process parameters on the current distribution in the slag pool is analyzed.

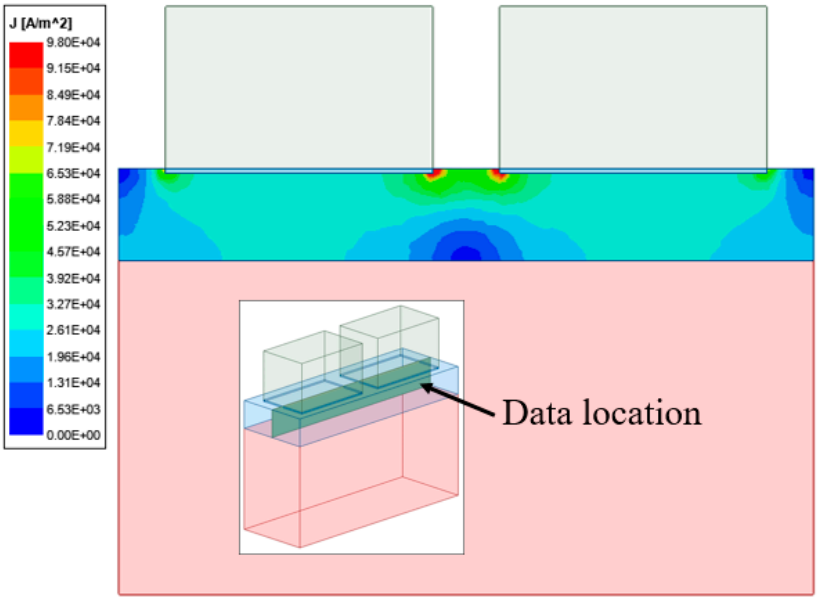



**Figure 6.** Current distribution on the positive longitudinal section of the slag pool.

### *4.3. The Influence of Process Parameters on the Current Distribution of the Model*

#### 4.3.1. The Influence of Current Frequency Variation on the Current Distribution

In this section, the influence of the current frequency on the current distribution is investigated by changing the current frequency of 10 Hz, 20 Hz, 30 Hz, 40 Hz and 50 Hz, respectively, while keeping the input power unchanged. Figure 7 shows the current distribution on the transverse center line of the upper surface of the slag pool at different current frequencies. It can be seen from the figure that with the increase in the current frequency, the current density distribution in the slag pool ($-1040$ mm $\leq$ X $\leq -900$ mm, $-100$ mm $\leq$ X $\leq$ 100 mm, 900 mm $\leq$ X $\leq$ 1040 mm) is basically unchanged. The current density in the outer side of the two electrodes ($-900$ mm $\leq$ X $\leq -620$ mm, 620 mm $\leq$ X $\leq$ 900 mm) decreases slightly with the increase in the current frequency. The current density in the inner side of the two electrodes ($-620$ mm $\leq$ X $\leq -100$ mm, 100 mm $\leq$ X $\leq$ 620 mm) increases significantly with the current frequency. When the current frequency increases from 10 Hz to 50 Hz, the maximum current density at the inner surface of the electrode increases from 166.9 kA/m$^2$ to 191.4 kA/m$^2$, an increase of 14.7%.

In order to focus on the analysis of the change in the current density with the current frequency in the slag pool, Figure 8 shows the current distribution on the transverse center line of the cross-section 20 mm from the top surface of the slag pool at different current frequencies. It can be seen from the figure that the current density in the slag pool does not change with the change in the current frequency. The current distribution in the corresponding area ($-900$ mm $\leq$ X $\leq -100$ mm, 100 mm $\leq$ X $\leq$ 900 mm) on the lower side of the electrode in the slag pool is relatively uniform. The following analysis focuses on the change in the current density in the slag pool.

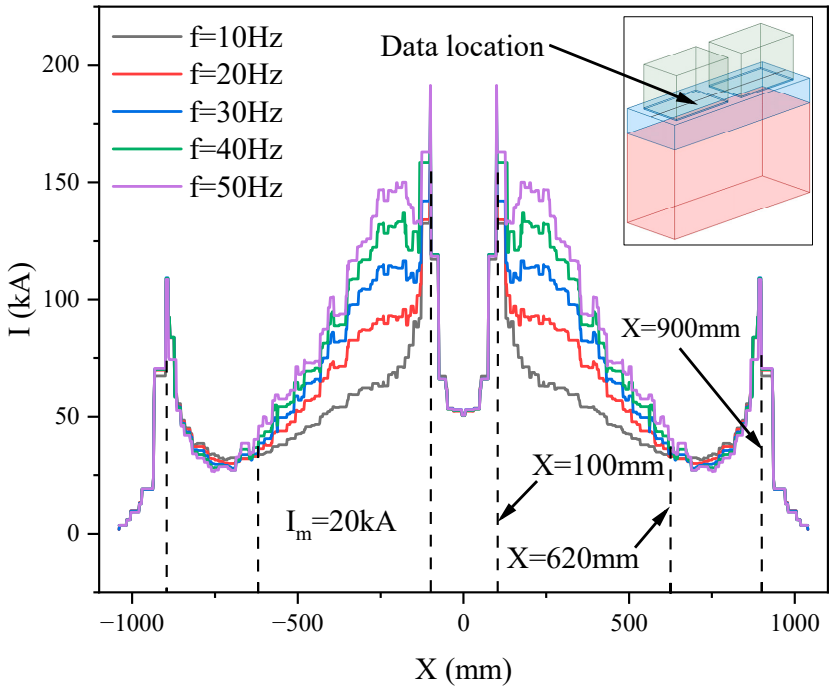



**Figure 7.** The current distribution on the transverse center line of the upper surface of the slag pool at different current frequencies.

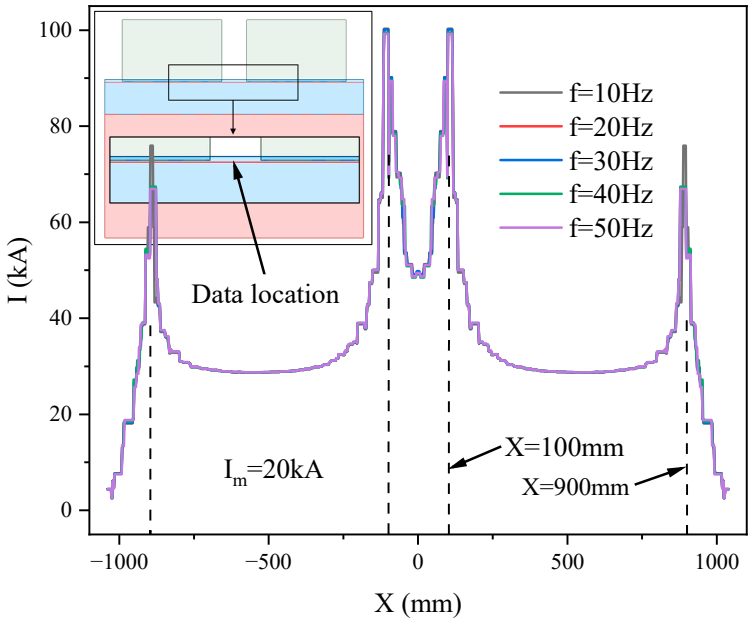



**Figure 8.** The current distribution on the transverse center line of the cross-section of 20 mm from the upper surface of the slag pool at different current frequencies.

#### 4.3.2. The Influence of Slag Pool Height Variation on the Current Distribution

In the process of electroslag remelting, the energy loss in the slag pool accounts for 50% to 60% of the total input energy. As the height of the slag pool increases, the energy loss will also increase. However, the slag pool is too shallow, the current and voltage fluctuations are large and the smelting process is unstable. In this section, the influence of the height of the slag pool on the current distribution of the slag pool is investigated by changing the height of the slag pool to 250 mm, 275 mm and 300 mm, respectively, while keeping the input power unchanged. Figure 9 shows the current distribution on the transverse center line of the cross-section at 20 mm from the upper surface of the slag pool at different heights of the slag

pool. It can be seen from the figure that the current distribution in the slag pool is basically the same when the height of the slag pool is different. The current density in the center and both sides of the slag pool ($-1040$ mm $\leq X \leq -900$ mm, $-100$ mm $\leq X \leq 100$ mm, 900 mm $\leq X \leq 1040$ mm) fluctuates, but there is not much change in the whole. The current density of the corresponding area ($-900$ mm $\leq X \leq -100$ mm, 100 mm $\leq X \leq 900$ mm) on the lower side of the electrode in the slag pool decreases with the increase in the height of the slag pool. The height of the slag pool increases from 250 mm to 300 mm, and the minimum current density in this area decreases from 29.5 kA/m$^2$ to 28.1 kA/m$^2$.

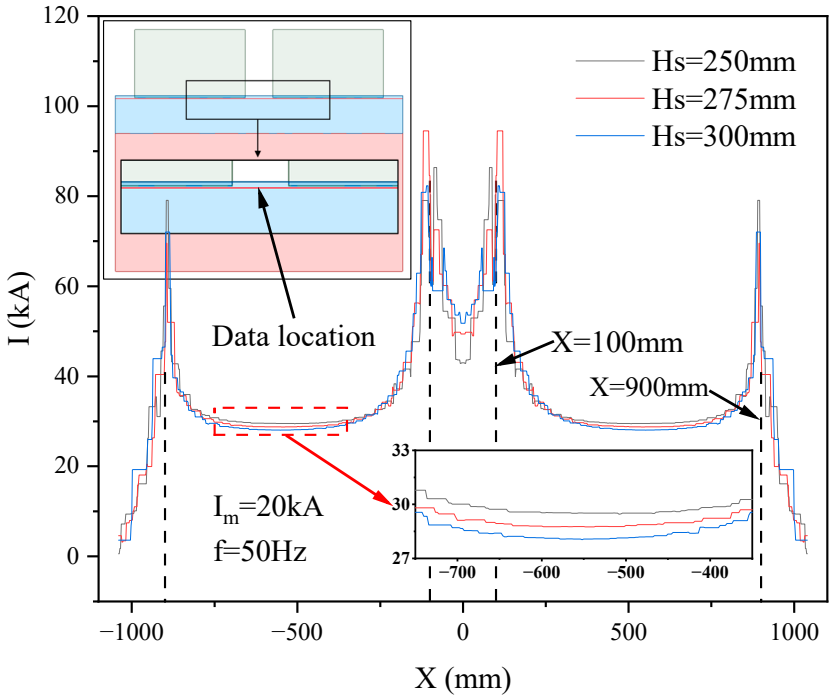



**Figure 9.** The current distribution on the transverse center line of the cross-section at 20 mm from the upper surface of the slag pool at different heights of the slag pool.

4.3.3. Effect of the Electrode Insertion Depth in the Slag on the Current Distribution

In this section, under the condition that the input power is constant, the depth of the slag pool is fixed at 275 mm, and the electrode insertion depth is changed to 10 mm, 15 mm and 20 mm, respectively; then, the influence of the electrode insertion depth on the slag pool current is studied. The current distribution on the transverse center line of the cross-section at 20 mm from the upper surface of the slag pool at different electrode slag insertion depths is shown in Figure 10. It can be seen from the figure that the current distribution in the slag pool is basically the same when the electrode is inserted into the slag pool at different depths. The current density in the center and both sides of the slag pool ($-1040$ mm $\leq X \leq -900$ mm, $-100$ mm $\leq X \leq 100$ mm, 900 mm $\leq X \leq 1040$ mm) did not change much. The current density of the corresponding area ($-900$ mm $\leq X \leq -100$ mm, 100 mm $\leq X \leq 900$ mm) on the lower side of the electrode in the slag pool decreases with the increase in the depth of the electrode inserted into the slag pool. The insertion depth increases from 10 mm to 20 mm, and the minimum current density in this area decreases from 29.4 kA/m$^2$ to 28.2 kA/m$^2$.

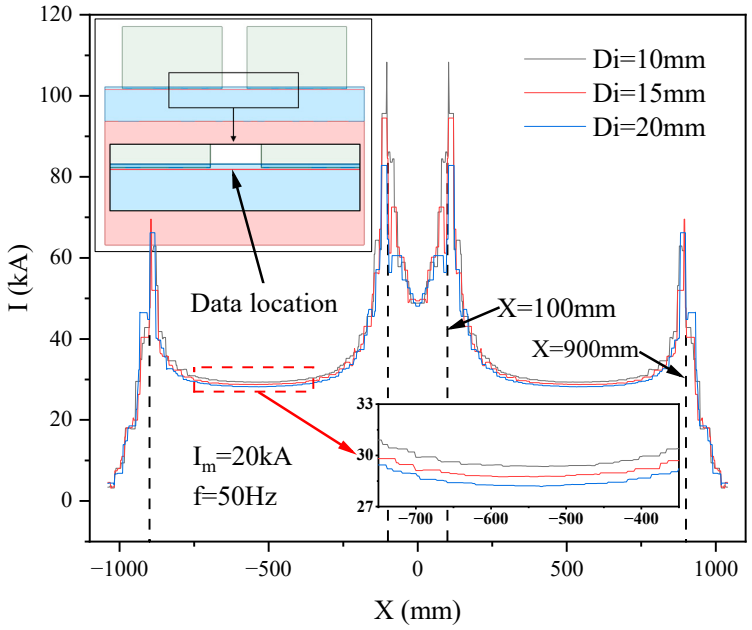



**Figure 10.** The current distribution on the transverse center line of the cross-section 20 mm from the top surface of the slag pool when there are different electrode insertion depths in the slag.

#### 4.3.4. Effect of the Ingot Height on the Current Distribution

As the smelting process progresses, the electrode gradually melts and shortens, and the ingot gradually solidifies. In this section, the influence of the ingot height on the current distribution of the slag pool was investigated by changing the ingot height of 500 mm, 1000 mm and 1500 mm, respectively, while keeping the input power unchanged. Figure 11 is the current distribution on the transverse center line of the cross-section at 20 mm from the upper surface of the slag pool at different ingot heights. It can be seen from the figure that the current distribution in the slag pool is basically the same when the ingot height is different. The current density distribution in the slag pool does not change with the change in the ingot height.

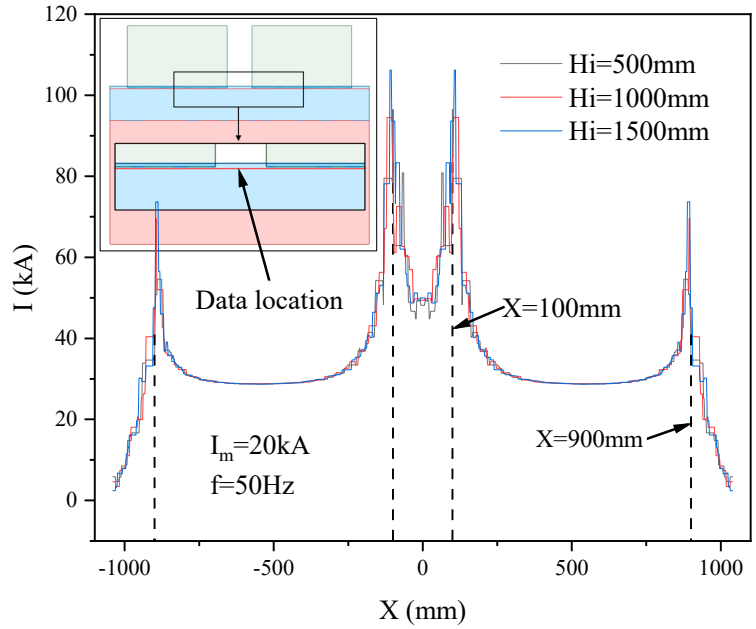



**Figure 11.** The current distribution on the transverse center line of the cross-section at 20 mm from the upper surface of the slag pool at different ingot heights.

## 5. Conclusions

(1) The accuracy of the calculation model is verified by comparing the calculated magnetic field strength data with the data measured by the Gauss meter.

(2) The Joule heat generated in the slag pool is much greater than that of the electrode and ingot; the maximum Joule heat is located at the contact between the electrode corner and the slag pool. The Joule heat density can reach 6.98 × 107 W/m$^3$, and the Joule heat near the middle of the two electrodes is greater than the rest.

(3) With the increase in the current frequency, the current density distribution in the slag pool is basically unchanged. The outer current density inside the two electrodes decreases slightly with the increase in the current frequency. The inner current density of the two electrodes increases significantly with the current frequency. When the current frequency increases from 10 Hz to 50 Hz, the maximum current density at the inner surface of the electrode increases from 166.9 kA/m$^2$ to 191.4 kA/m$^2$. The current distribution in the corresponding area of the lower side of the electrode in the slag pool is relatively uniform.

(4) The current density in the center and both sides of the slag pool does not change with the height of the slag pool and the depth of the electrode inserted into the slag pool. The current density of the corresponding area on the lower side of the electrode in the slag pool decreases with the increase in the height of the slag pool and the depth of the electrode inserted into the slag pool. The current density distribution in the slag pool does not change with the change in the ingot height.

**Author Contributions:** Simulations, formal analysis and validation, Q.L. and Z.J. Review, editing and experiments, Q.L. Conceptualization, supervision and project administration, Y.S. All authors have read and agreed to the published version of the manuscript.

**Funding:** This research received no external funding.

**Data Availability Statement:** Data are contained within the article.

**Conflicts of Interest:** Author Qi Li was employed by the company Shanghai Electric SHMP Casting & Forging Co., Ltd. The remaining authors declare that the research was conducted in the absence of any commercial or financial relationships that could be construed as a potential conflict of interest.

## References

1. Li, Z. Reviewing the past and looking forward to the future for electroslag metallurgy. *Spec. Steel* **1999**, *20*, 1–6.
2. Li, Z. Development process, current situation and trends of electroslag metallurgy. *J. Mater. Metall.* **2011**, *10*, 1–7.
3. Kharicha, A.; Karimi-Sibaki, E.; Wu, M.; Ludwig, A.; Bohacek, J. Review on modeling and simulation of electroslag remelting. *Steel Res. Int.* **2018**, *89*, 1700100. [CrossRef]
4. Campbell, J. A Future for Vacuum Arc Remelting and Electroslag Remelting—A Critical Perspective. *Metals* **2023**, *13*, 1634. [CrossRef]
5. Wang, Y.; Gao, G. Features and application of electroslag metallurgy process. *Metall. Equip.* **2010**, *S1*, 54–56.
6. Li, C.; Xu, Y.; Han, D.; Fan, G.; Yang, C. Study on properties of 18MND5 steel forgings for PWR steam generator. *J. Phys. Conf. Ser.* **2021**, *2085*, 012034. [CrossRef]
7. Wang, L.; Liu, F.; You, L.; Zeng, X.; Hu, Y. Safety evolution and investigation of dynamic strain aging effect on tensile property of 18MND5 low alloy steel used in nuclear island equipment. *At. Energy Sci. Technol.* **2018**, *52*, 1831.
8. Liu, X.; Wang, J.; Jia, W.; Gao, J.; Zhao, L.; Tang, Z. Modeling electroslag remelting process of large ingot for nuclear power station and its application. *Foundry* **2010**, *59*, 1315–1319.
9. Dong, Y.; Jiang, Z.; Liu, H.; Chen, R.; Song, Z. Simulation of multi-electrode ESR process for manufacturing large ingot. *ISIJ Int.* **2012**, *52*, 2226–2234. [CrossRef]
10. Li, B.; Wang, B.; Tsukihashi, F. Modeling of electromagnetic field and liquid metal pool shape in an electroslag remelting process with two series-connected electrodes. *Metall. Mater. Trans. B* **2014**, *45*, 1122–1132. [CrossRef]
11. Tong, W.; Li, W.; Zang, X.; Li, H.; Jiang, Z.; Li, D. A Comprehensive Mathematical Model of Electroslag Remelting with Two Series-Connected Electrodes Based on Sequential Coupling Simulation Method. *Metals* **2020**, *10*, 658. [CrossRef]
12. Hernandez-Morales, B.; Mitchell, A. Review of mathematical models of fluid flow, heat transfer, and mass transfer in electroslag remelting process. *Ironmak. Steelmak.* **1999**, *26*, 423–438. [CrossRef]
13. Weber, V.; Jardy, A.; Dussoubs, B.; Ablitzer, D. A comprehensive model of the electroslag remelting process: Description and validation. *Metall. Mater. Trans. B* **2009**, *40*, 271–280. [CrossRef]

14. Wei, J.; Ren, Y. Mathematical simulation of magnetic field in ESR system. *Acta Metall. Sin.* **1995**, *31*, 51–60.
15. Dong, Y.; Jiang, Z.; Li, Z. Mathematical model for electroslag remelting process. *J. Iron Steel Res. Int.* **2007**, *14*, 7–12. [CrossRef]
16. Jardy, A.; Ablitzer, D.; Wadier, J.F. Magnetohydronamic and thermal behavior of electroslag remelting slags. *Metall. Trans. B* **1991**, *22*, 111–120. [CrossRef]
17. Xia, Z.; Sun, Z.; Zhang, M.; Lin, W.; Zheng, T.; Shen, Z.; Ding, B.; Liu, C.; Lu, H.; Lei, Z.; et al. Numerical Investigation about the Effect of Axial Static Magnetic Field on Improvement of Metal Pool Profile During Electroslag Remelting Process. *Metall. Mater. Trans. B* **2023**, *54*, 3101–3114. [CrossRef]
18. Duan, Y.; Li, B.; Liu, Z.; Huang, X.; Li, D.; Wang, F. Numerical study on the effect of low-frequency power supply on desulfurization in the electroslag remelting process. *Steel Res. Int.* **2023**, *94*, 2300081. [CrossRef]
19. Liu, Y.; Zhang, Z.; Li, G.; Wang, Q.; Wang, L.; Li, B. Effect of Current on Structure and Macrosegregation in Dual Alloy Ingot Processed by Electroslag Remelting. *Metals* **2017**, *7*, 185. [CrossRef]
20. Hugo, M.; Dussoubs, B.; Jardy, A.; Jessica, E.; Poisson, H. Influence of the mold current on the electroslag remelting process. *Metall. Mater. Trans. B* **2016**, *47*, 2607–2622. [CrossRef]
21. Igizianova, N.A.; Sokolova, E.V. Modeling electromagnetic processes in direct current electroslag remelting. *Int. J. Adv. Manuf. Technol.* **2021**, *113*, 3189–3193. [CrossRef]
22. Wang, F.; Wang, Q.; Baleta, J.; Li, B. Sequentially Coupled Simulation of Multiphysical Fields During Twin-Electrode Electroslag Remelting Process. *Metall. Mater. Trans. B* **2020**, *51*, 2285–2297. [CrossRef]
23. Huang, X.; Duan, Y.; Liu, Z.; Li, B.; Wang, F. Role of Electrode Rotation on Improvement of Metal Pool Profile in Electroslag Remelting Process. *Metals* **2021**, *11*, 1675. [CrossRef]
24. Liu, F.; Li, Y.; Jiang, Z.; Li, H.; Geng, X.; Chen, X. Electromagnetic behavior for laboratory scale and industrial scale electroslag remelting process. *J. Cent. South Univ. (Sci. Technol.)* **2015**, *46*, 3580–3585.
25. Wang, F.; Li, B. Analysis of electromagnetic field and joule heating of electroslag remelting processes. *Acta Metall. Sin.* **2010**, *46*, 794–799. [CrossRef]
26. Liu, Y.; He, Z.; Liu, S.; Liu, Z.; Xia, T.; Wang, F.; Li, B. Numerical simulation of electromagnetic, flow and temperature fields in electroslag remelting process. *Chin. J. Process Eng.* **2014**, *14*, 16–22.
27. Jing, X.; Jiang, Z.; Liu, F.; Chen, X.; Duan, J. Numerical simulation of electric and temperature fields for ESR hollow ingot with current conductive mold. *J. Mater. Metall.* **2013**, *12*, 203–208.
28. Li, B.; Wang, F.; Tsukihashi, F. Current, magnetic field and joule heating in electroslag remelting processes. *ISIJ Int.* **2012**, *52*, 1289–1295. [CrossRef]
29. Wang, C.; Ge, F.; Zhang, Y.; Wang, D.; Luo, W.; Wan, H. Influence of process parameters on solidification process in electroslag remelting. *Foundry Technol.* **2013**, *34*, 1321–1323.
30. Patel, A.D. Electrode immersion depth effects in the ESR process. In Proceedings of the 2011 International Symposium on Liquid Metal Processing and Casting, Nancy, France, 25–28 September 2011.
31. Wang, X.; Li, Y. Numerical simulation of electromagnetic field and temperature field of ESR. *J. Northeast. Univ. (Nat. Sci.)* **2014**, *35*, 813–818.
32. Sibaki, E.K.; Kharicha, A.; Wu, M.; Ludwig, A.; Holzgruber, H.; Ramprecht, M. A numerical study on the influence of the frequency of the applied AC current on the electroslag remelting process. In Proceedings of the 2013 International Symposium on Liquid Metal Processing & Casting, Austin, TX, USA, 22–25 September 2013; Springer International Publishing: Cham, Switzerland, 2016; pp. 13–19.


**Disclaimer/Publisher's Note:** The statements, opinions and data contained in all publications are solely those of the individual author(s) and contributor(s) and not of MDPI and/or the editor(s). MDPI and/or the editor(s) disclaim responsibility for any injury to people or property resulting from any ideas, methods, instructions or products referred to in the content.